Common offset ground penetrating radar data inversion based on ray theory

XUE Meiqi[1]   LIU Sixin[1*]   LU Qi[1]   LI Hongqing[1]   WANG Yuanxin[1]
CHANG Xinghao[2]   RAN Limin[2]   ZHAO Yonggang[2] and LI Jianwei[2]

1. *College of Geo-Exploration Science and Technology Jilin University Changchun 130026 China;*
2. *North China Petroleum Engineering Company SINOPEC Zhengzhou 457000 China*

Abstract：The authors use the common offset ground penetrating radar（GPR）data inversion based on ray theory to estimate interval velocity and to obtain the relative permittivity. In the ray-tracing based inversion the input data are the offset distance between antennas the velocity of the first layer the pick-up amplitude and reference amplitude of each reflection layer. The thickness and velocity of each layer are calculated by this recursive method. Firstly the horizontal homogeneous layered medium model is established and the ideal inversion results are obtained. Subsequently Monte Carlo method is used to establish a randomly undulating homogeneous layered medium model. The common offset GPR data for the built geological model is then simulated by finite-difference time-domain（FDTD）. It proved that this ray-tracing based inversion method is feasible for the horizontal layered geological model even the layered geological model with random undulation. Undulation represented by *RMS* height and CL（correlation length） influences the inversion results. Finally a more complex geological model—pinch-out model was established. In the pinch-out model the pinch-out interface can be clearly identified though there is a false anomaly which will not significantly affect the identification of the underground medium structure.

Keywords：ray-tracing based inversion; FDTD; rough surface; common offset; GPR data; reflection amplitude

0　Introduction

GPR is a high-resolution geophysical technology based on electromagnetic wave propagation in the frequency range between 1 MHz and 3 GHz（Forte *et al.* 2014）. It is used for the internal imaging of various types of geological materials such as soil rocks and artificial materials including concrete and asphalt（Mostapha *et al.* 2018; Fa 2013）. It has the advantages of high speed high resolution continuity

and no damage and therefore it has been widely used in geological prospecting archaeology roadbed detection etc. （Cassidy & Millington 2009; Zyada *et al.* 2011）. The path electromagnetic field strength and waveform of electromagnetic waves when propagating in the medium vary with the dielectric properties and geometry of the medium through which they pass. Therefore based on the recorded electromagnetic wave travel time amplitude and other waveform data the geometry of the target body and shape of abnormal

structure can be interpreted. In seismic processing velocity models are usually obtained by analyzing the data collected at multiple source-receiver offsets (Forte *et al.* 2014). However most commercial GPR systems are equipped with a single receiver antenna so the acquisition of multiple offset data sets is very demanding (Forte *et al.* 2014; Pipan *et al.* 1999). GPR data collection in common offset is simple fast and can be used for large-scale survey along the gird or line. The obtained data show the change of the physical properties of the underground medium within a certain range. Therefore we can use the common offset GPR data to estimate velocity.

1 Method

1. 1 Monte Carlo method for stochastic rough surface modeling

Using the power spectral density the random rough surface can be simulated and generated by the Monte Carlo method which is also called the linear filtering method. The basic idea of Monte Carlo method is to filter it with power spectrum in frequency domain and to get the height fluctuation of rough surface by inverse fast Fourier transform (IFFT). The *RMS* height and the *CL* are the two most basic and important parameters in the simulation of rough surfaces which have a great influence on the height and frequency of rough surfaces (Salvarezza *et al.* 2019).

Fig. 1 shows the samples of random rough surface under different *RMS* height and *CL*. When the *CL* is the same the greater the *RMS* height the greater the undulation degree of rough surface. When the *RMS* height is fixed the smaller the *CL* the more severe the rough surface transformation that is the smaller the change period. It can be seen that *RMS* height and the *CL* relate to the scale of the rough surface in the vertical and the horizontal direction respectively.

(a) Rough surface corresponding to different *RMS* height with the same *CL* (2 m); (b) rough surface corresponding to different *CL* with the same *RMS* height (0. 1 m).

Fig. 1 Rough surface corresponding to different *CL* (a) and *RMS* height (b)

1. 2 Forward method based on FDTD

In the field of computational electromagnetics (EM) FDTD method is one of the most popular numerical techniques for solving EM wave propagation problems (Craig *et al.* 2019). FDTD method differentiates Maxwell equation in time domain and space domain (Taflove & Umashankar 1989). Using leapfrog method to calculate the electric and magnetic fields alternately in space domain and the change of electromagnetic field is simulated by updating in time domain to achieve numerical calculation.

FDTD decomposes the forward target into a Yee unit and forms a staggered network with Yee's unit (Yee 1966; Shaari *et al.* 2010; Luebbers *et al.* 1993). The electric and magnetic field components are placed crosswise in space and the relative spatial position of each component is also suitable for the difference calculation of Maxwell's equation which

can properly describe the propagation characteristics of electromagnetic field. At the same time the electric and magnetic fields are alternately sampled in time (Soldovieri *et al.* 2007) and the sampling interval is half a time step apart so that the Maxwell curl equation is discretized to form an explicit difference equation which can be solved iteratively in time without the need for matrix inversion. Therefore given the initial conditions of the corresponding electromagnetic problem FDTD can gradually obtain the distribution of the spatial electromagnetic field at each time.

FDTD method is relatively simple in concept accurate for any complex model (Irving & Knight 2006; Balanis 1989). This paper uses MATLAB code based on FDTD and PML absorbing boundary provided by Irving and Knight (2006).

1.3 Inversion method based on geometric ray theory

The ray-tracing based inversion method used in this paper was proposed by Forte *et al.* (2014). We assume that the propagation signal is a plane EM wave. Near each trace location the underground medium is assumed to be homogeneous isotropic non-magnetic ($\mu_r = 1$) non-conductive ($\sigma = 0$) and non-dispersible (Davis & Annan 1989). The changes of antenna coupling inherent attenuation and scattering effect are ignored. Normal GPR surveys are performed in transverse electric (TE) broadside configuration (Jol 2009). Therefore we only consider the TE mode. According to these assumptions the proposed method requires offset (x) velocity of the first layer medium (v_1) amplitude of direct wave (A_{i1}) amplitude of reflected wave (As_i) and travel time (TWT_i).

Given the first layer velocity (v_1) offset (x) and travel time of the first layer (TWT_1) we can get the thickness of the first layer (h_1) by Equation (1):

$$h_1 = \frac{1}{2}\sqrt{(v_1 TWT_1)^2 - x^2} \qquad (1)$$

Then the angle of incidence is obtained by Equation (2):

$$\theta_1 = \text{Arctan}\left(\frac{x}{2h_1}\right) \qquad (2)$$

Using the amplitude values picked up (As_1 and Ai_1) the reflection coefficient of the first layer R_1 can be obtained by Equation (3):

$$R_1 = \frac{As_1}{Ai_1} \qquad (3)$$

Then Snell equation gives the velocity of GPR signal in the second layer:

$$v_2 = \frac{\sin(\theta_2)}{\sin(\theta_1)}v_1 \qquad (4)$$

Where θ_2 is obtained by rearranging the Fresnel equation of TE mode (Balanis 1989):

$$\theta_2 = \text{Arctan}\left(\frac{1+R_1}{1-R_1}\tan\theta_1\right) \qquad (5)$$

If we know the thickness of the first $n-1$ layers the GPR signal velocities of the first n layers and the TWT_n of the nth interface reflected wave then the thickness of the nth layer (h_n) is the only positive solution of the following third-degree equation (Forte *et al.* 2014):

$$ah_n^3 + bh_n^2 + ch_n + d = 0 \qquad (6)$$

$$a = \frac{4}{v_n} \qquad (7)$$

$$b = \frac{4}{v_n^2}\sum_{i=1}^{n-1}v_i h_i + 8\sum_{i=1}^{n-1}\frac{h_i}{v_i} \qquad (8)$$

$$c = \frac{x^2}{v_n} + \frac{8}{v_n}\left(\sum_{i=1}^{n-1}v_i h_i\right)\left(\sum_{i=1}^{n-1}\frac{h_i}{v_i}\right) +$$
$$4v_n\left(\sum_{i=1}^{n-1}\frac{h_i}{v_i}\right)^2 - v_n TWT_n^2 \qquad (9)$$

In horizontally layered media the incident angle of the kth interface is equal to the transmitted angle of the $(k-1)^{th}$ interface. Such angle (θ_k) is related to the horizontal projection ($\triangle x_k$) of the travel path in the kth layer through the following equation (Fig. 2):

S represents the transmitter R represents the receiver x is the offset h_i and v_i are the thicknesses and EM velocities of the layers respectively θ_i and $\triangle x_i$ are the incident angles and the horizontal projections of the travel path respectively.

Considering the small value of θ_k and the Snell's equation we obtain:
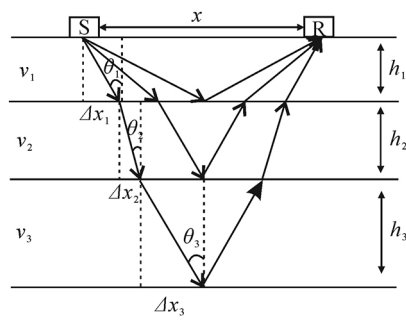
Fig. 2   Schematic diagram of electromagnetic wave ray path in horizontally layered media

$$\triangle x_k = \frac{v_k h_k}{v_{k-1} h_{k-1}} \triangle x_{k-1} \quad (11)$$

According to geometric conditions:

$$\sum_{i=1}^{n} \triangle x_i = \frac{x}{2} \quad (12)$$

Then we can use the Fresnel equation for TE antenna configuration to calculate the first $n-1$ reflection and transmission coefficients relative to the nth reflected wave:

$$R_k = \frac{\sin(\theta_{k+1} - \theta_k)}{\sin(\theta_{k+1} + \theta_k)} \quad (13)$$

$$T_k = 1 + R_k \quad (14)$$

with $k = 1 \ 2 \ \cdots \ n - 1$.

Considering the symmetry of the travel path (Fig. 2) and using the above coefficients and amplitudes we picked (As_n and Ai_1) the incident and reflected amplitudes of the nth interface can be obtained by the follow equation:

$$Ai_n = \prod_{i=1}^{n-1} T_i \quad (15)$$

$$Ar_n = \frac{As_n}{\prod_{i=1}^{n-1} (2 - T_i)} \quad (16)$$

Then the reflection coefficient of the nth interface is given by:

$$R_n = \frac{Ar_n}{Ai_n} \quad (17)$$

The velocity in the $(n+1)^{\text{th}}$ layer is given by the Snell's equation:

$$v_{n+1} = \frac{\sin(\theta_{n+1})}{\sin(\theta_n)} v_n \quad (18)$$

with

$$\theta_{n+1} = \text{Arctan}\left(\frac{1 + R_n}{1 - R_n} \tan\theta_n\right) \quad (19)$$

By iterating this method for all the interpreted reflections in a GPR trace the thicknesses and velocities of all the imaged layers can be obtained.

2   Numerical examples

First we established a horizontal homogeneous layered medium model with a size 10 m × 4. 5 m. The specific parameters are shown in Table 1.

Table 1   Model parameters for forward modeling

Layer	Relative permittivity	Velocity / m · (ns)$^{-1}$	Layer thickness / m
1	5	0. 1342	2. 0
2	7	0. 1134	0. 5
3	10	0. 0949	0. 5
4	12	0. 0867	1. 5

Then numerical simulation is performed on the established model. The frequency of transmitting antenna is 100 MHz. The time window is 120 ns and the sampling interval is 0. 04 ns. The starting position of transmitting antenna is 0. 5 m and the ending position is 8. 5 m. The starting position of receiving antenna is 1. 0 m and the ending position is 9. 0 m. The moving step of both antennas is 0. 25 m.

After obtaining the forward results we pick up the reflection amplitude; perform the above iterative inversion on data of all traces. The calculated results are shown in Table 2.

Table 2   Inversion results of layered models

Data type	Layer 1 Thickness / m	Layer 1 Velocity / m · (ns)$^{-1}$	Layer 2 Thickness / m	Layer 2 Velocity / m · (ns)$^{-1}$	Layer 3 Thickness / m	Layer 3 Velocity / m · (ns)$^{-1}$	Layer 4 Thickness / m	Layer 4 Velocity / m · (ns)$^{-1}$
Numerical model	2. 0000	0. 134	0. 5000	0. 1134	0. 5000	0. 0949	1. 5	0. 0867
Calculate result	2. 0103	–	0. 5146	0. 1143	0. 5263	0. 0978	–	0. 0907
Relative error / %	0. 5150	–	2. 9200	0. 7900	5. 2600	3. 0500	–	4. 6100

It can be seen from the above table that the relative error will increase with depth but the relative error of this method is not more than 6% so this ray-tracing based inversion method is feasible.

Then we established three undulating stratum models with a size 10 m × 5 m with the same *CL* and different *RMS* heights. The length of each rough interface is 15 m. The specific parameters are shown in models 1–3 of Table 3.

After obtaining the forward results we pick up the reflection amplitude perform the above iterative inversion on all traces and perform linear interpolation on the space between the two tracks   the numerical model and calculated result are shown in Fig. 3.

Table 3   Model parameters of undulating strata for forward modeling

Model	Relative permittivity				*CL*/m	*RMS*/m
	Layer 1	Layer 2	Layer 3	Layer 4		
1	5	10	15	20	10	0.4
2	5	10	15	20	10	0.3
3	5	10	15	20	10	0.2
4	5	10	15	20	3	0.1
5	5	10	15	20	4	0.1
6	5	10	15	20	6	0.1
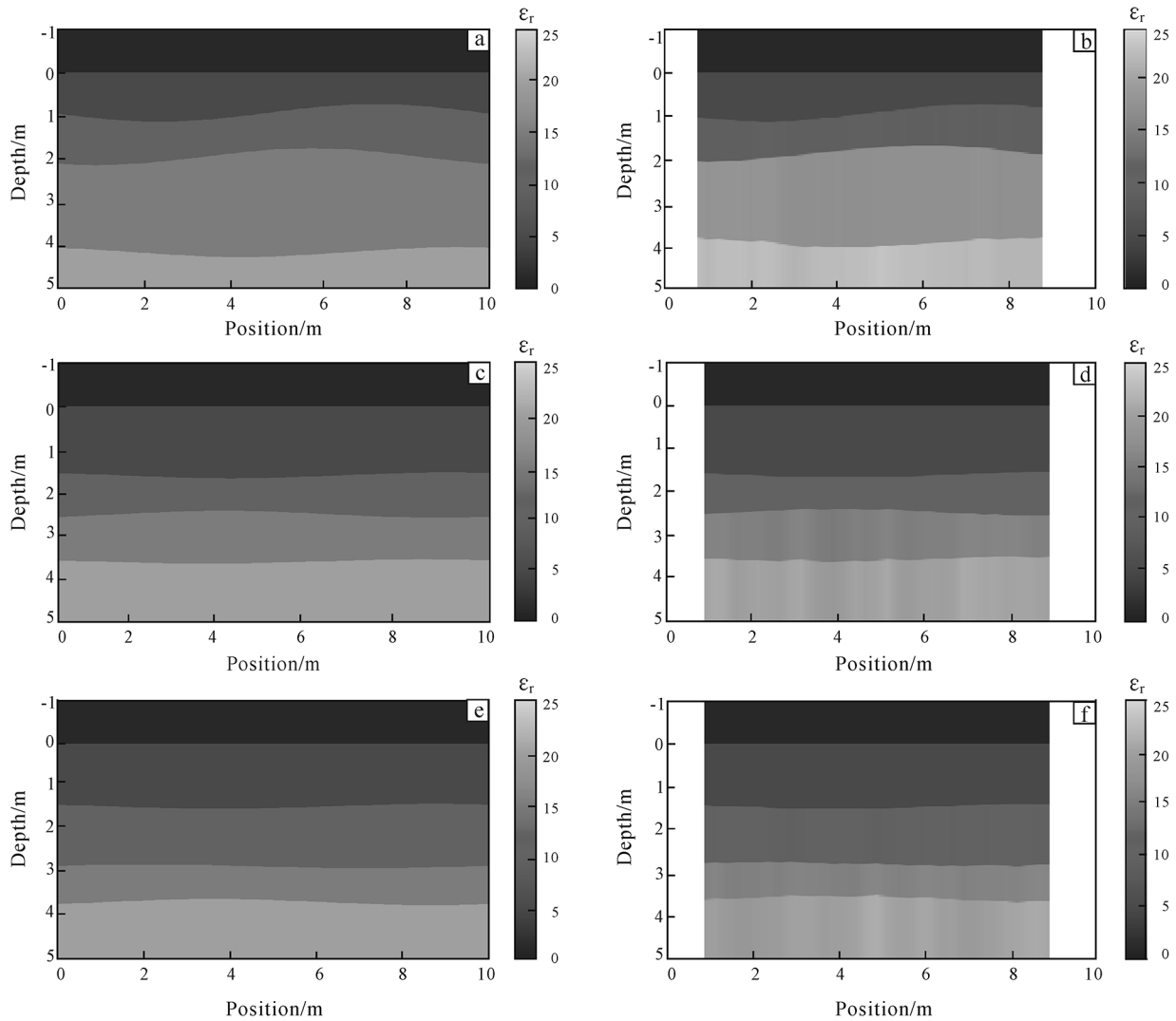
（a）（c）and（e）are numerical models *RMS* are 0.4 m 0.3 m and 0.2 m respectively;（b）（d）and（f）are calculated models *RMS* are 0. 4 m 0.3 m and 0.2 m respectively.

Fig. 3   Three undulating strata models with the same *CL*

The top layer of the models is air. The transmitting and receiving antennas are located at 0 m on the *y*-axis. Due to the position setting of transmitting antenna and the receiving antenna we can only calculate the dielectric constant of the medium between 0.75–8.75 m.

It can be seen from above examples that this ray-tracing based inversion method can be used for the inversion of common offset GPR data. It can perfectly distinguish the shape and position of the reflection interface but as the *RMS* increases in other words the degree of undulation of the rough surface increa-

the calculation error of the permittivity of the medium is also increasing.

Subsequently we established three undulating stratum models with the same *CL* heights and different correlation length. The specific parameters are shown in models 4–6 of Table 3.

The numerical model and calculated result are shown in Fig. 4.

It can be seen from above examples as the correlation length increases the calculation error of the permittivity of the medium is also decreasing.
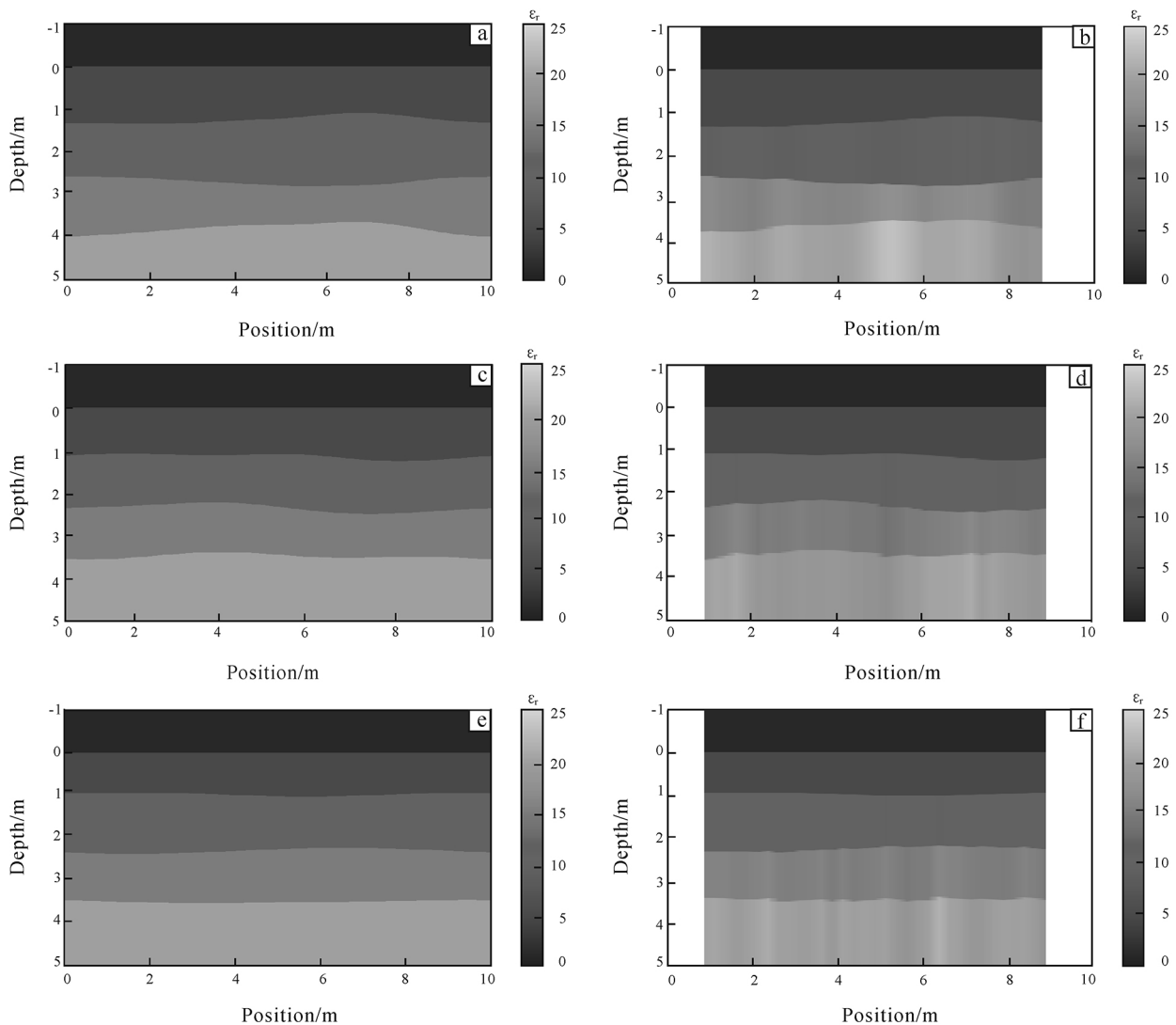
（a）（c）and（e）are numerical models *CL* are 3 m 4 m and 6 m respectively;（b）（d）and（f）are calculated models *CL* are 3 m 4 m and 6 m respectively.

Fig. 4　Three undulating stratum models with the same *RMS* heights

Finally we established a pinch-out model with an inclination of 30 degrees the numerical model and calculated result are shown in Fig. 5.

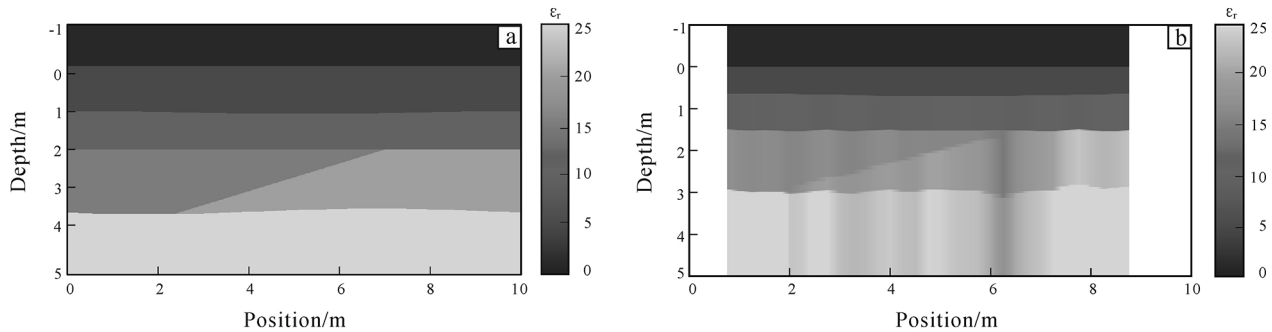From Fig. 5 the pinch-out interface can be clearly seen in the inversion results. However there is an obvious false anomaly in the dielectric constant where the pinch-out strata disappeared (6.2 m). The main reason is that the diffraction wave at this place is obvious and it is very difficult to pick up the amplitude of the reflected wave. Anyway this false anomaly does not affect our identification on the true structure of the underground medium.

Fig. 5 Diagrams of numerical pinch-out model (a) and calculated pinch-out model (b)

3　Conclusion

It is proven that the ray-tracing based inversion is feasible in the horizontal homogeneous layered medium model even in the layered geological model with random undulation. In the horizontal homogeneous layered medium model the error will increase with depth. In the layered geological model with random undulation as the *RMS* increases that is the degree of undulation of the reflection interface increases the calculation error of the permittivity of the medium is also increasing. As the correlation length increases that is the degree of undulation of the reflection interface decreases the calculation error of the permittivity of the medium is also decreasing. In the pinch-out model the pinch-out interface can be clearly identified although there is a false anomaly which will not significantly affect the identification of the underground medium structure. In general it is feasible to use this method to invert common offset ground penetrating radar data.

References

Balanis C A. 1989. Advanced engineering electromagnetics. s. l. : Wiley 981.

Cassidy N J Millington T M. 2009. The application of finite-difference time-domain modelling for the assessment of GPR in magnetically lossy materials. *Journal of Applied Geophysics* **67**: 296-308.

Craig W Antonios G Alan G *et al.* 2019. A CUDA-based GPU engine for gprMax: Open source FDTD electromagnetic simulation software. *Computer Physics Communications* **237**: 208-218.

Davis J L Annan A P. 1989. Ground-penetrating-radar for high-resolution mapping of soil and rock stratigraphy. *Geophysical Prospecting* **37**(5): 531-551.

Fa W Z. 2013. Simulation for ground penetrating radar (GPR) study of the subsurface structure of the Moon. *Journal of Applied Geophysics* **99**: 98-108.

Forte E Dossi M Pipan M *et al.* 2014. Velocity analysis from common offset GPR data inversion: Theory and application to synthetic and real data. *Geophysical Journal Internal* **197**(3): 1471-1483.

Irving J Knight R. 2006. Numerical modeling of ground-penetrating radar in 2-D using MATLAB. *Computers & Geosciences* **32**(9): 1247-1258.

Jol H M. (ed.) 2009. Ground penetrating radar: theory and applications. s. l. : Elsevier Science 524.

Luebbers R Steich D Kunz K. 1993. FDTD calculation of scattering from frequency-dependent materials. *IEEE Transactions on Antennas and Propagation* **41**(9): 1249-1257.

Mostapha A M M Alsharahi G Driouach A. 2018. 2D FDTD

Simulation of ground penetrating radar imaging under sub-surface with two different antenna types. *Procedia Manu-facturing* **22**: 420-427.

Pipan M Baradello L Forte E *et al.* 1999. 2-D and 3-D processing and interpretation of multi-fold ground penetrating radar data: A case history from an archaeological site. *Journal of Applied Geophysics* **41**(2/3): 271-292.

Salvarezza R C Alonso C A Vara J M *et al.* 2019. The electrochemical growth mode of metal overlayers: A Monte Carlo simulation applicable to the effect of foreign adatom on roughness development. *Journal of the Electrochemical Society* **138**(10): 2938-2942.

Shaari A Ahmad R S Chew T H. 2010. Effects of antenna-target polarization and target-medium dielectric contrast on GPR signal from non-metal pipes using FDTD simulation.

NDT & E International **43**(5): 403-408.

Soldovieri F Hugenschmidt J Persico R *et al.* 2007. A linear inverse scattering algorithm for realistic GPR applications. *Near Surface Geophysics* **5**(1): 29-41.

Taflove A Umashankar K. 1989. Review of FD-TD numerical modeling of electromagnetic wave scattering and radar cross-section. *Proceedings of the IEEE* **77**(5): 682-699.

Yee K S. 1966. Numerical solution of initial boundary value problems involving Maxwell's equations in isotropic media. *IEEE Transactions on Antennas and Propagation* **14**: 302-307.

Zyada Z Matsuno T Hasegawa Y *et al.* 2011. Advances in GPR-based landmine automatic detection. *Journal of the Franklin Institute* **348**: 66-78.